Weak Fault Enhancement Method for Bearing Fault Diagnosis by Using Stochastic Resonance

Zhang Chao[1], Duan Haoran[1], Wang Jianguo[1], Li Jianjun[2], Zhang Biao[1], Ma Yunting[1]

(1. School of Mechanical Engineering, Inner Mongolia University of Science and Technology, Baotou 014010, China)

(2. School of Information Engineering, Inner Mongolia University of Science and Technology, Baotou 014010, China)

***Abstract*—large mechanical equipment is subject to periodic vibrations in harsh operating environments for a long time. Bearing failure produces violent changes in the behavious of large rotating machinery as the safety and reliability of the scene. Therefore, it is especially significant to effectively identify the early failure of the bearing. Since the signal of bearing fault belongs to a low-frequency weak fault, it is hard to classify the characteristic frequency. In order to solve this shortcoming, a new stochastic resonance model, which is established on the joint Woods-Saxon and monostable potential well, is presented and used to strengthen the characteristics frequency, also the bearing fault characteristic frequency is gained. The simulation analysis shows that the proposed method can effectively extract the weak fault characteristics which are submerged in the noise environment, and the bearing test proves that it can be used to strengthen and extract the fault characteristics frequency.**

Keywords—bearing failure; signal extraction; stochastic resonance

I. INTRODUCTION

Since the Italian researcher Benzi[1] who proposed Stochastic resonance (SR) in 1981, SR has attracted the attention of many scholars and has been widely used in image enhancement[2], mechanical equipment fault diagnosis[3], etc. field. Feng Yi[4] raised an adaptive multi-stationary cascaded stochastic resonance (AMCSR) signal enhancement method, it was based on the classic bistable SR model, to effectively extract weak fault signals. Cao Yanlong[5] suggested a variable-scale SR method to extract and identify the weak impact signals which are under the intensive background buzz. Ji Yuandong[6] was on the basis of the power function SR model to study the influence of different potential well parameters on the system. Leng[7] proved that the variable-scale SR eliminates the influence of the small parameter limitation using stochastic resonance. Du[8] use the method of numerically to research the SR in an underdamped quartic double-well potential under the time-delayed feedback conditions, the results show that the delay time and damping coefficient would impact on the SR. Chen[9] investigated the relationship of location and depth in the triple-well potential on the condition of vibrational resonance. It proved that by changing the depth and situation of the wells can obtain the greatest vibrational resonance. Zhang[10] has further explored a novel SR paradigm, which named multi-scale bistable array and planned a new approach to detect the feeble signal based on this paradigm. Qiao[11] planned an unsaturated SR model, which overcomes the trouble of inherent saturation of potential function in classical SR and is successfully set for the fault diagnosis of gearboxes and bearings.

Inspired by the literature [11], this paper uses the Woods-Saxon to transform the power function monostable SR system into a new bistable SR structure. This new SR structure is used to enhance the feeble fault frequency and attain the purpose of catching the bearing fault signal characteristic frequency. And this method is verified by simulation signals and actual bearing fault signal analysis, respectively.

II. POTENTIAL MODEL

A. Woods-Saxon Potential Model

The Woods-Saxon [12] is a nonlinear symmetric potential which can be expressed as follows:

$$U_{ws}(x) = -\frac{a}{1+exp((|x|-b)/c)} \tag{1}$$

Where a forces the depth of potential, b controls the breadth of potential, and c dominates the precipitousness of potential, in equation 1.

As shown in Fig. 1, the shape of the Woods-Saxon potential function is controlled by adjusting the values of the variables a, b and c. From Fig. 1, that when the values of a and b are immovable also the scale of c is changed, it can be observed that with the value of c increases, the steepness of the potential function also changes gentle, and implied the variable c decides the wall precipitousness. Similarly, it can be seen that the depth of the potential has replaced, while the b and c values are fixed, and the value of a is adjusted. Also fixing the a and c values, and regulating the value of the b. We can notice that as b becomes larger, the width of the well also increasing. In summary, the effects of the parameters on the potential function in the Woods-Saxon are independent. This has the advantage of avoiding the coupling of parameters in the traditional potential function.

B. Monostable Potential

Monostable potential well function [13] SR model which can be illustrated as follows:

$$\dot{x}(t) = -U'_m(x) + S(t) + n(t) \tag{2}$$

Here $\dot{x}(t)$ is the derivative of the system output $x(t)$, $S(t)$ represents the input signal, $n(t)$ stands the Gaussian white noise with means of 0 and the variance equals D,

978-1-7281-0860-5/19/$31.00 ©2019 IEEE

$U'_m(x)$ represents the derivative of the monostable potential function $U_m(x)$.

$$U_m(x) = -g\,x + \frac{e}{4}x^4 \tag{3}$$

Here variables *g* and *e* belong to system variables and they are real numbers. With the change of variables *g* and *e*, the ship of $U_m(x)$ image changes, as is shown in Fig. 2.

C. *Joint Woods-Saxon and Monostable Potential*

We planed a novel bistable potential mode *MWS*, by the way of linking the Woods-Saxon potential together with the monostable potential. As is shown in Fig. 3 (in this case *a*=1, *b*=0.2, *c*=0.5, *g*=0.001, *e*=0.01), and the novel bistable potential *MWS* is illustrated as follows:

$$U_{mws}(x) = U_m(x) - U_{ws}(x) = -gx + \frac{e}{4}x^4 + \frac{a}{1+exp\left(\left(|x|-b\right)/c\right)} \tag{4}$$

The novel potential function $U_{mws}(x)$ contains five parameters *a*, *b*, *c*, *g*, *e* and there is no coupling relationship between the parameters. Therefore, the figure of *MWS* potential well is changed easily by adjusting each element to make it a bistable or monostable model to match different input signal requirements. In summary, the *MWS* has the advantages of both the bistable potential function and the monostable potential function, which can be used to process weak periodic signals.

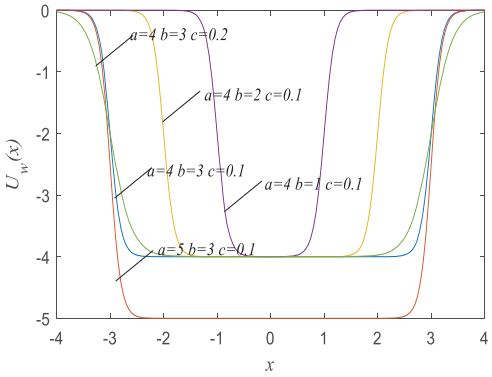

Fig. 1. Shap of Woods-Saxon potential $U_w(x)$ with different parameters

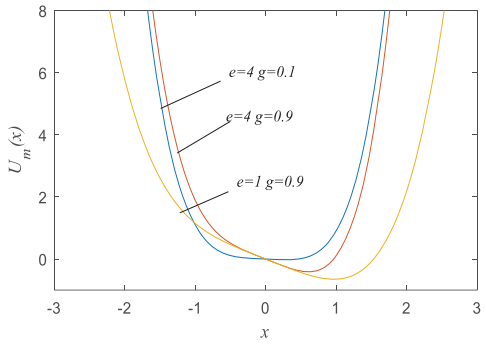

Fig. 2. Shap of Monostable potential $U_m(x)$ with different parameters

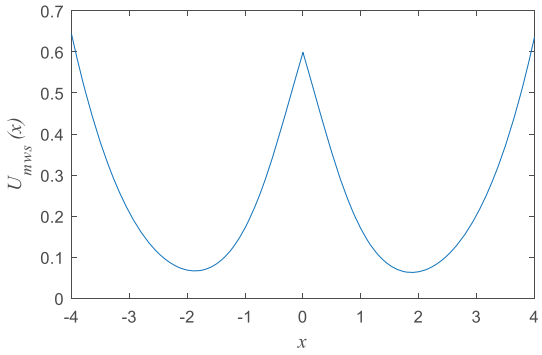

Fig. 3. Shap of joint Monostable and Woods-Saxon potential $U_{mws}(x)$ with *a*=1, *b*=0.2, *c*=0.5, *e*=0.01, *g*=0.001.

III. STOCHASTIC RESONANCE SYSTEM

A. *Classical Stochastic Resonance Model*

Stochastic resonance (SR) phenomenon needs three basic conditions which are (1) a nonlinear system, (2) a kind of strepitus that is built in system or joins into the coherent input, and (3) a week coherent input signals [14]. The classical SR system is described [15] as:

$$\frac{dx}{dt} = -\frac{dU(x)}{dx} + A\sin\left(2\pi f_0 t + \varphi\right) + n(t) \tag{5}$$

Where *A* represents the weak periodic signal amplitude, and f_0 is driving frequency of the weak periodic signal, $n(t)$ is Gaussian white noise that meets the following characteristics:

$$\begin{cases} n(t) = 0 \\ n(t)\,n(t-\tau) = 2D\delta(t) \end{cases} \tag{6}$$

where *D* stands the noise intensity.

$U(x)$ represents the reflection-symmetric quartic potential, both *a* and *b* are real parameters. It can be written as follows:

$$U(x) = -\frac{a}{2}x^2 + \frac{b}{4}x^4 \tag{7}$$

Substituting (7) to (5), the traditional function of SR can be described as:

$$\frac{dx}{dt} = ax - bx^3 + A\sin\left(2\pi tf_0 + \varphi\right) + n\left(t\right) \tag{8}$$

B. *Joint Woods-Saxon and Monostable Stochastic Resonance*

We changed the traditional model into novel one *MWS*. The equation of *MWS* is illustrated as follows:

$$U'_{mws}\left(x\right) = -\frac{a}{c}sgn\left(x\right)exp\left(\frac{\left|x\right|-b}{c}\right)\left(1+exp\left(\frac{\left|x\right|-b}{c}\right)\right)^{-2} + A\sin\left(2\pi tf_0 + \varphi\right) + \eta\left(t\right) + g - ex^3 \tag{9}$$

$$sgn\left(x\right) = \begin{cases} 1 & x > 0 \\ 0 & x = 0 \\ -1 & x < 0 \end{cases} \tag{10}$$

Here *sgn(x)* represents the sign function. From equation (9) can conclude that the system output depends on the input signal and the potential function model. Compared with the equation (5), the *MWS* SR is different from the conventional SR only in the potential model. In addition, the input signal, the system, and random noise simultaneously determine the generation of SR phenomenon. In practical situations, periodic driving strength and noise strength are immovable. Therefore, the validity of the SR system mostly depends on the potential strength, and a suitable potential model shape can effective amplification of the weak fault signal.

IV. SIMULATED SIGNAL ANALYSIS

For the sake of proving the joint potential function can achieve SR phenomenon, and detect weak signals. We set the simulation signal *S(t)* for verification analysis, and the simulation signal settings are shown in equation (11):

$$S\left(t\right) = A\sin\left(2\pi tf_e\right) \tag{11}$$

Where, A=0.2, the sampling frequency f_s=10 Hz, and the sampling point number N is taken as 5000, set fault frequency f_e=0.002 Hz and added signal with noise intensity of 0.8 in time-domain. Fig. 4 is a time-domain diagram of the simulated signal *S(t)*. Obviously, *S(t)* is already engulfed in the heavy noise and the law of simulated signal cannot be observed at all. After processing by the *MWS* SR system (in this case *a*=2, *b*=0.01, *c*=0.02, *g*=0.00001, *e*=2.2). the time-domain diagram dealt with *MWS* can clearly observe the regularity of input signal, as shown in Fig. 5. In addition, the frequency-domain diagram is shown in Fig. 6. And Fig. 7 shows a partial magnification of the frequency-domain diagram after *MWS* processing. From Fig. 7 it can be clearly observed that the frequency of the simulated signal is 0.002 Hz.

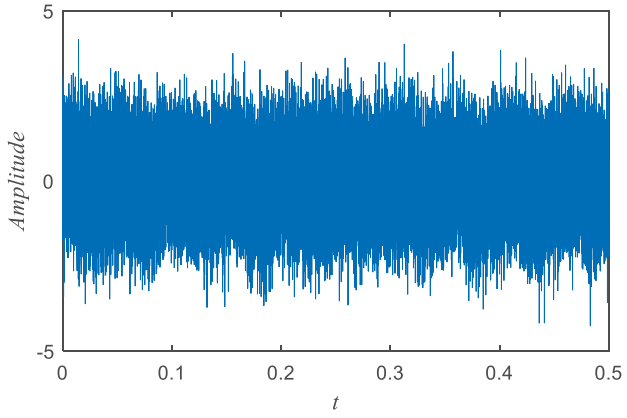

Fig. 4. The time waveform of simulation signal

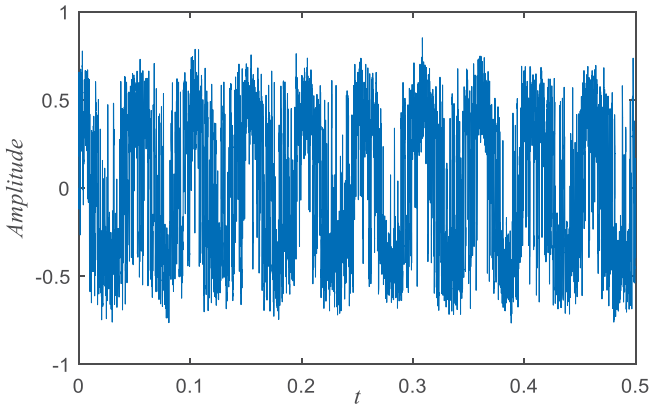

Fig. 5. Output signal after processing by the proposed method for the simulation signal.

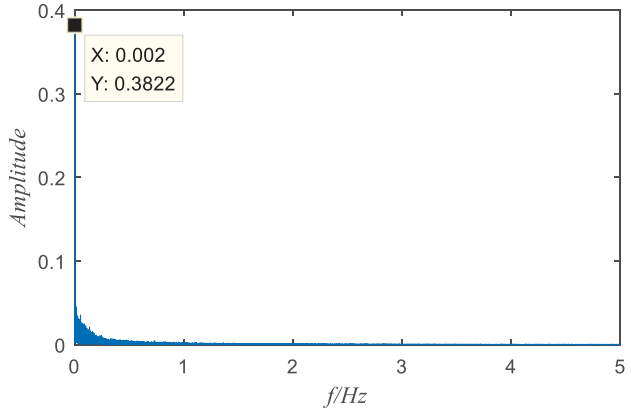

Fig. 6. Output frequency after processing by the proposed method for the simulation signal.

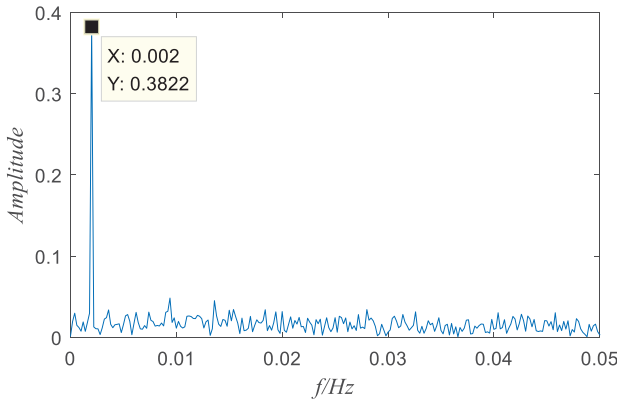

Fig. 7. Partial magnification of the output frequency

V. EXPERIMENTAL VERIFICATION IN BEARING FAULT DIAGNOSIS

In this part of the experiment, the vibration signals used originated from Inner Mongolia University of Science and Technology. The test bench model used is the HZXT-DS-003 double-span and double-rotor rolling bearing test bench, as shown in Fig. 8. The bearing type used is 6205-2RS deep groove ball bearing. Moreover, the acceleration sensors which are mounted on the motor drive end, supporting the shaft base and the fan end, respectively. From left to right in Fig. 8 there is three-phase induction motor, torque sensor, and dynamometer. In particular, the sampling frequency f_s=12000 Hz, the sampling point N=12000, the bearing pitch diameter is 39.04mm, and the rolling element pitch diameter is 7.94mm, the contact angle is 0°, the number of rolling elements is 9, and the bearing rotation speed is 1797r/ min.

Fig. 8. HZXT-DS-003 double-span and double-rotor rolling bearing test bench.

By calculation, we can see that the bearing natural frequency theoretical value is 30 Hz, and the theoretical value of the outer ring fault is 107.31 Hz. The time-domain and frequency-domain diagrams are shown in Fig. 9 and Fig. 10, respectively. It can be observed that the frequency of the fault is completely submerged due to the interference of the background noise. It is hard to identify fault information in the domain and frequency domain waveforms. So, the fault signal is input into the new potential function model *MWS* (in this case a=2950.101, b=19.1502, c=75.5003, g=0.00001, e=19.53) to get the time domain diagram as shown in Fig. 11, the frequency domain diagram is shown in Fig. 12. From the time domain diagram Fig. 11 proves that the impact signal is partially suppressed after signal processing. From the frequency domain diagram Fig. 12 noticed that the amplitude at the fault frequency f=108 Hz is significantly improved, indicating that the *MWS* system enhances the energy of the fault frequency. In other words, the energy of the interference noise is suppressed, and it is proved that the *MWS* can improve the fault characteristic frequency to get the detection of the bearing fault signal. Considering the signal is derived from reality and the signal source is complex, there is a slight diversity between the actually detected characteristic frequency and the theoretical characteristic frequency value.

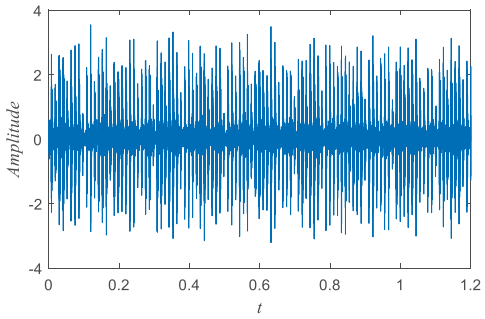

Fig. 9. The vibration signal time domain diagram of bearing outer ring

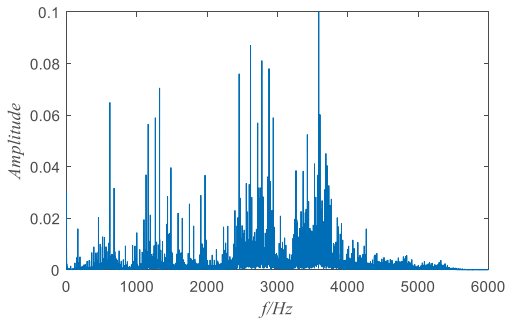

Fig. 10. The vibration signal frequency domain diagram of bearing outer ring

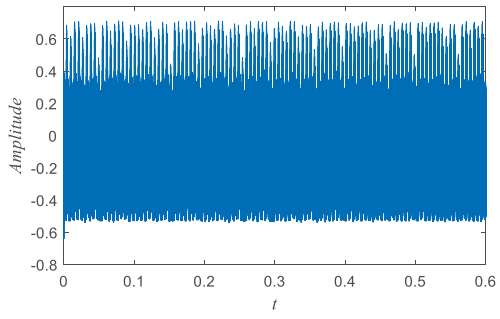

Fig. 11. Output signal after processing by the proposed method for bearing outer ring signal.

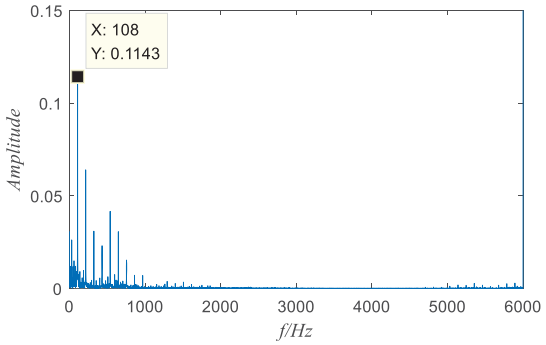

Fig. 12. Output frequency after processing by the proposed method for bearing outer ring signal.

VI. CONCLUSION

It is especially important to effectively identify the early failure of the bearing，which has a major effect on the process of large rotating machinery. Since the bearing fault is a weak fault, and the fault characteristic frequency often neglects by the way of using the conventional methods. In this paper, the *MWS* SR model is used to improve the energy of the fault characteristic frequency and obtain the characteristic frequency. Moreover, it is verified by the experimental data. Finally, this article provides an idea for bearing fault diagnosis.

ACKNOWLEDGMENT

This research is supported by National Science Foundation of China (NSFC) (No. 51565046), Natural Science Foundation of Inner Mongolia Autonomous Region, China (No. 2018KG007), Inner Mongolia Higher Education Youth Science and Technology Leadership Talent Project (NJYT-18-A10).

REFERENCES

[1] R. Benzi, G. Parisi, and S. A. Vulpiani. "A Theory of Stochastic Resonance in Climatic Change," SIAM Journal on Applied Mathematics , 43.3, 1983, pp. 565-578.

[2] N. Kojima, B. Lamsal, N. Matsumoto, and M. Yamashiro, “Proposing Autotuning Image Enhancement Method Using Stochastic Resonance,” Electronics and Communications. Japan, 2019, pp:35-46

[3] H. Yuanyuan, Z. Chao, and C. Shuai, "The Application of Self-adaptive Stochastic Resonance and ELMD in Bearing Fault Diagnosis," Mechanical Science and Technology for Aerospace Engineering ,37.4, 2018, pp: 607-613.

[4] F. Yi, L. Baochun, and Z. Dengfeng, “Bearing Weak Fault Signal Detection Based on Adaptive Multi-stable Stochastic Resonance,” Vibration. Testing and Diagnosis, 36.6, 2016, pp: 1168-1174+1240-1241.

[5] C. Yanlong, Y. Biyu, Y. Jiangxin, Z. Shipu, and Z. Weijie, "Impact Signal Adaptive Extraction and Recognition Based on scale transformation Stochastic Resonance System," JOURNAL OF VIBRATION AND SHOCK, 35.5, 2016, pp: 65-69.

[6] J. Yuandong, Z. Lu, and L. Maokang, "Generalized stochastic resonance of power function type single-well system." Acta Physica Sinica, 63.16, 2014, pp:164302-164302.

[7] F. Shengbo, W. Taiyong, L. Yonggang, and W. Wenjin, "Detection of Weak Periodic Impact Signals Based on Scale Transformation Stochastic Resonance," China Mechanical Engineering,17.4, 2006, pp:387-390.

[8] D. Luchun, and D. C. Mei, "Stochastic resonance, reverse-resonance and stochastic multi-resonance in an underdamped quartic double-well potential with noise and delay," Physica A Statistical Mechanics & Its Applications ,390.20,2011, pp:3262-3266.

[9] C. Zhijuan, and L. Ning, "Impact of depth and location of the wells on vibrational resonance in a triple-well system," Pramana , 90.4,2018, pp:49.

[10] Z. Xiaofei, H. Niaoqing, "Multi-scale bistable stochastic resonance array: A novel weak signal detection method and application in machine fault diagnosis," Science China. Technological Sciences , 56.9,2013, pp:2115-2123.

[11] Q. Zijian, Y. Lei, L. Jing, "An adaptive unsaturated bistable stochastic resonance method and its application in mechanical fault diagnosis," Mechanical Systems and Signal Processing, 84, 2017, pp:731-746.

[12] Lu, Siliang , Q. He , and F. Kong , "Stochastic resonance with Woods–Saxon potential for rolling element bearing fault diagnosis." Mechanical Systems and Signal Processing, 45.2, 2014, pp:488-503.

[13] L. Jimeng, C. Xuefeng, and H.Zhengjia, "Adaptive Monostable Stochastic Resonance Based on PSO with Application in Impact Signal Detection," Journal of Mechanical Engineering 47(21), 2011, pp: 58-63

[14] Y. Yuangen, Y. Lijian, and W. Canjun, "Subthreshold Periodic Signal Detection by Bounded Noise-Induced Resonance in the FitzHugh–Nagumo Neuron." Complexity ,2018, 2018, pp:1-10

[15] Q. Zijian,” Research and Application of Weak Signal Detection Method Based on Stochastic Resonance Theory,” Lanzhou University of Technology: Academic, 2015